Materials Research Bulletin 72 (2015) 245–251

Contents lists available at ScienceDirect

Materials Research Bulletin

journal homepage: www.elsevier.com/locate/matresbu

Color tunable emission and energy transfer of Ce^{3+} and Tb^{3+} co-doped novel $La_6Sr_4(SiO_4)_6F_2$ phosphors with apatite structure

Qingfeng Guo [a], Libing Liao [a,*], Maxim S. Molokeev [b,c], Lefu Mei [a,*], Haikun Liu [a]

[a] Beijing Key Laboratory of Materials Utilization of Nonmetallic Minerals and Solid Wastes, National Laboratory of Mineral Materials. School of Materials Sciences and Technology, China University of Geosciences, Beijing 100083, China
[b] Laboratory of Crystal Physics, Institute of Physics, SB RAS, Krasnoyarsk 660036, Russia
[c] Department of Physics, Far Eastern State Transport University, Khabarovsk 680021, Russia

ARTICLE INFO

Article history:
Received 28 January 2015
Received in revised form 17 June 2015
Accepted 22 July 2015
Available online 26 July 2015

Keywords:
Inorganic compounds
Luminescence
Phosphors
Crystal structure
Optical properties

ABSTRACT

Single-phase $La_6Sr_4(SiO_4)_6F_2$: Ce^{3+}, Tb^{3+} samples with apatite-like structure have been synthesized via solid-state reaction method. The phase structure, luminescence properties, lifetime, the PL thermal stability, as well as the fluorescence decay curves of the samples were investigated to characterize the resulting samples. Effective energy transfer occurs from Ce^{3+} to Tb^{3+} in $La_6Sr_4(SiO_4)_6F_2$, which shows more intense Blue-Green light under UV light excitation. In addition, a possible mechanism of the energy-transfer from Ce^{3+} to Tb^{3+} ion is also proposed. The critical distance R_C of Ce^{3+} to Tb^{3+} ions in $La_6Sr_4(SiO_4)_6F_2$ host was calculated to be 11.878 Å. All the results indicate that $La_6Sr_4(SiO_4)_6F_2$:Ce^{3+}, Tb^{3+} phosphors have potential applications to be used as near UV-convertible phosphors for white light-emitting diodes.

1. Introduction

It is known to us that white light-emitting diodes (*w*-LEDs) have attracted increasing attentions from scientists and engineers attributed to their advantages compared to the traditional incandescent bulbs and fluorescent lamp, such as low power consumption, high luminescence efficiency, environment-friendly, as well as good stability in physical and chemical properties [1–4]. It is reported that the conventional way to fabricate white LEDs is based on a combination of blue LED and yellow phosphor of $Y_3Al_5O_{12}$:Ce^{3+} (YAG:Ce) [5,6]. However, there are some shortcomings of such *w*-LEDs based on the combination such as low color rendering index (CRI) and highly correlated color temperature [7,8]. In order to improve the CRI value, a combination of a near ultraviolet (*n*-UV) LED chip (350–420 nm) with red, green, and blue-emitting phosphors has been widely investigated in recent years [9–11]. Therefore it is necessary to find new phosphors to be excited by *n*-UV light. The activation of rare earth ions for their 4f→4f or 5d→4f transitions plays an important and irreplaceable role in lighting and display fields [12–14], among which the Ce^{3+} ion with broad band has been widely investigated as a highly efficient activator due to the transition between the $4f^1$ ground state and the crystal field components of the 5d excited state configuration [15,16]. In addition, Tb^{3+} could be also an important emitting activator for phosphors with sharp green lines. However, the Tb^{3+} ion has only weak absorption bands in the range of 300–400 nm due to the 4f→4f absorption transitions [17]. It is well known that interesting luminescence behaviors occur by energy transfer from sensitizer to activator in many hosts [18,19]. Therefore, it is logical to enhance the emission intensity and obtain broad-band excitation in the near ultraviolet (n-UV) region by co-doping Ce^{3+} and Tb^{3+}.

Apatite have been widely used as host lattices in recent years, and rare earth ions doped apatite phosphors can exhibit luminescence properties owing to their excellent stability and compatibility with efficient luminescent properties in n-UV LEDs [20,21]. The apatite family can be represented with a general formula of $M_{10}(TO_4)_6X_2$ (M = Na^+, K^+, Ca^{2+}, Sr^{2+}, Mn^{2+}, Ce^{3+}, Y^{3+}, La^{3+} etc. and T = P^{5+}, S^{6+}, Si^{4+}, etc. and X = F^-, Cl^-, Br^-, OH^-, O^{2-} etc.) crystallizing in the hexagonal system with space group $P6_3/m$. Apatite-type compound consists of two cationic sites, that is, 4*f* (C_3 point symmetry) with a nine-fold coordinated site and 6 h (C_s point symmetry) with a seven-fold coordinated site, respectively. In general, fluoride-containing apatites doped with rare-earth ions have great potential application in solid state lighting for their adjustable luminescence properties due to the introduce of fluoride ions in the host lattice, such as $Ca_8NaLa(PO_4)_6F_2$:Eu^{2+},Mn^{2+} [22], $Ba_2Y_3[SiO_4]_3F$:Ce^{3+} [23], $Ba_3NaLa(PO4)_3F$:Eu^{2+},Mn^{2+} [24].

* Corresponding authors. Tel./fax: +86 1082331701.
E-mail address: clayl@cugb.edu.cn (L. Liao).

http://dx.doi.org/10.1016/j.materresbull.2015.07.029
0025-5408/

Recently phosphors with apatite structure for w-LEDs application have been widely developed, such as $Ca_{10}(SiO_4)_3(SO_4)_3F_2$:$Eu^{2+}$ [25], $La_6Ba_4(SiO_4)_6F_2$:Ce^{3+}, Tb^{3+} [26], $Ca_2Gd_8(SiO_4)_6O_2$:Eu^{3+} [27], $Ca_9Mg(PO_4)_6F_2$:Eu^{2+}, Mn^{2+} [28]. However, there are no researches on $La_6Sr_4(SiO_4)_6F_2$ (LSSF) phosphors were found in the previous literatures.

Accordingly, in this paper, the crystal structure, luminescence properties as well as the energy transfer behaviors between Ce^{3+} and Tb^{3+} ions in LSSF crystal lattice have been investigated in detail. In addition we get intense blue-green phosphor which can be efficiently excited by n-UV LEDs.

2. Experimental

2.1. Synthesis procedures

A series of $La_6Sr_4(SiO_4)_6F_2$:Ce^{3+},Tb^{3+} phosphors were prepared by a traditional high temperature solid-state reaction. $SrCO_3$ (Aldrich, 99.9%), SiO_2 (Aldrich, 99.9%), NH_4HF_2 (Aldrich, 99.9%), CeO_2 (Aldrich, 99.995%), La_2O_3 (Aldrich, 99.995%), and Tb_4O_7 (Aldrich, 99.995%) were used as starting materials. The starting materials were mixed and ground according to the given stoichiometric ratio firstly. After all materials were ground thoroughly in an agate mortar, the mixture was pre-heated at 600 °C for 3 h in air atmosphere in alumina crucibles with covers. After cooling to room temperature, the preliminary products were placed into an alumina crucible and were heated at 1350 °C for 4 h in a reducing atmosphere with flowing gas (10% H_2 + 90% N_2) with the flow rate of 0.5 L/min. Then the products were cooled to room temperature naturally. Finally, the products were ground again into powder for further analysis.

2.2. Characterization

Phase structures of the as-prepared samples were examined by X-ray powder diffractometer (D/max-rA 12 kW, Japan) with Cu Kα radiation (λ = 1.5418 Å) from 10° to 70°(2θ). The step scanning rate (2θ values ranging from 5° to 100°) used in Rietveld analysis was 3 s/step with a step size of 0.02°. Rietveld refinement was obtained using the computer software TOPAS [29]. Room temperature Photoluminescence excitation (PLE) and emission (PL) spectra were measured on a fluorescence spectrophotometer (F-4600, HITACHI, Japan) with a photomultiplier tube operating at 450 V, and a 150 W Xe lamp was used as the excitation lamp. In addition, the temperature-dependence luminescence properties were measured on the same spectrophotometer combined with a self-made heating attachment and a computer-controlled electric furnace. The decay curves of Ce^{3+} lifetime values were recorded on a spectro-fluorometer (HORIBA JOBIN YVON FL3-21) with the 370 nm pulse laser radiation (370-nm Nano LED, model number 08254) used as excitation source.

3. Results and discussion

3.1. Crystal structure

The powder diffraction data of $La_6Sr_4(SiO_4)_6F_2$ for Rietveld analysis was collected at room temperature with a D/max-rA powder diffractometer radiation. It can be seen that almost all XRD patterns of $La_6Sr_4(SiO_4)_6F_2$ were indexed by hexagonal cell ($P6_3/m$) with parameters close to $La_6Ba_4(SiO_4)_6F_2$ [30]. Therefore crystal structure of $La_6Ba_4(SiO_4)_6F_2$ was taken as starting model for Rietveld refinement. The concentrations of La and Sr ions in sites were refined with assumption that sum occupancies in each site equal to 1. Refinement was stable and gives low R-factors (Table 1, Fig. 1). Besides, the lattice constants of $La_6Sr_4(SiO_4)_6F_2$ are calculated as $a = b = 9.8549(3)$ Å, $c = 7.3022(3)$ Å, and $V = 614.174\ (2)$ Å^3. Small reliability parameters (Table 1) verify the phase purity of the as-prepared sample. The inset of Fig. 1 shows the structure of $La_6Sr_4(SiO_4)_6F_2$ compound. The Si atoms are tetrahedrally coordinated forming [SiO_4] groups, which are isolated from each other. As shown in the inset of Fig. 1, the structure of LSSF offers two types of nonequivalent crystallographic sites for various cations to occupy, which are the 4*f* (C_3) site with nine-coordination La(1)/Sr(1) and the 6*h* (C_s) site with seven-coordination La(2)/Sr(2)). According to the effective ionic radii and charge balance, Ce^{3+}/Tb^{3+} ions prefer to occupy the sites of La^{3+}. In addition, the ionic radiuses of coordinated Ce^{3+}/Tb^{3+} ions are similar to that of La^{3+} in either seven- or nine-fold coordination in LSSF crystal lattice, which can be seen in Table 2 [31].

Table 1
Main parameters of processing and refinement of the $La_6Sr_4(SiO_4)_6F_2$ sample.

Compound	$La_6Sr_4(SiO_4)_6F_2$
Space group	$P6_3/m$
a, Å	9.8549(3)
c, Å	7.3022(3)
V, Å^3	614.17(4)
2θ-interval,	5–100
Number of reflections	235
Number refined parameters	46
R_{wp}, %	10.68
R_p, %	7.86
R_{exp}, %	7.06
χ^2	1.51
R_B, %	3.77

Fig. 2 shows the characterization of phase homogeneity of the selected as-prepared LSSF: 0.07Ce^{3+}, *y*Tb^{3+} (*y* = 0, 0.01, 0.03 and 0.07) and LSSF: 0.07Tb^{3+} samples, and the standard data for $La_6Ba_4(SiO_4)_6F_2$ (ICSD card no. 170852) is shown as a reference. It is found that all the representative XRD patterns of as-prepared samples matched well with that of standard $La_6Ba_4(SiO_4)_6F_2$ phase (ICSD card no. 170852), which indicates that all the as-prepared LSSF: Ce^{3+}, Tb^{3+} samples have hexagonal apatite structure with the space group of $P6_3/m$ and that the doping of Ce^{3+} and Tb^{3+} did not cause any detectable change in the crystal lattice. In addition, the

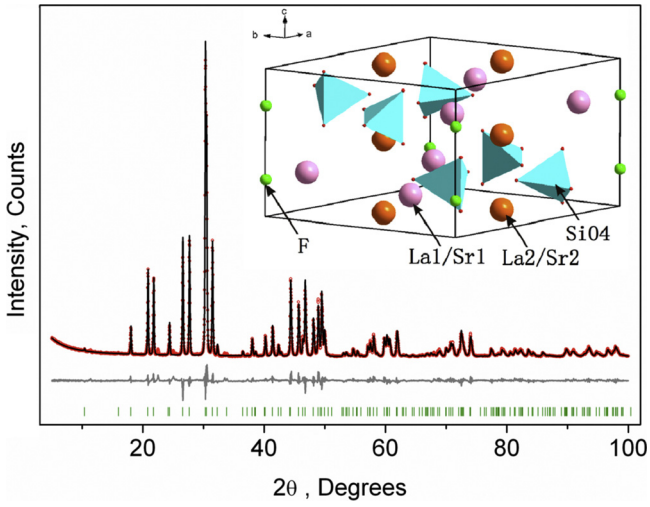

Fig. 1. Rietveld analysis patterns for X-ray powder diffraction data of $La_6Sr_4(SiO_4)_6F_2$. The solid black lines are calculated intensities, and the red dots are the observed intensities. The gray solid lines below the profiles stand for the difference between the observed and calculated intensities. The short green vertical lines show the position of Bragg reflections of the calculated pattern. The inset shows the crystal structure diagram of $La_6Sr_4(SiO_4)_6F_2$.

Table 2
Structure parameters of LSSF and ionic radius (Å) for given CNs of La^{3+}, Sr^{2+}, Tb^{3+}, and Ce^{3+} ions.

Ion	Sites	Symmetry	Ionic radius (Å) CN = 9	Ionic radius (Å) CN = 7
La^{3+}	4f/6h	C_3/C_S	1.216	1.10
Sr^{2+}			1.31	1.21
Tb^{3+}			1.095	0.98
Ce^{3+}			1.196	1.07

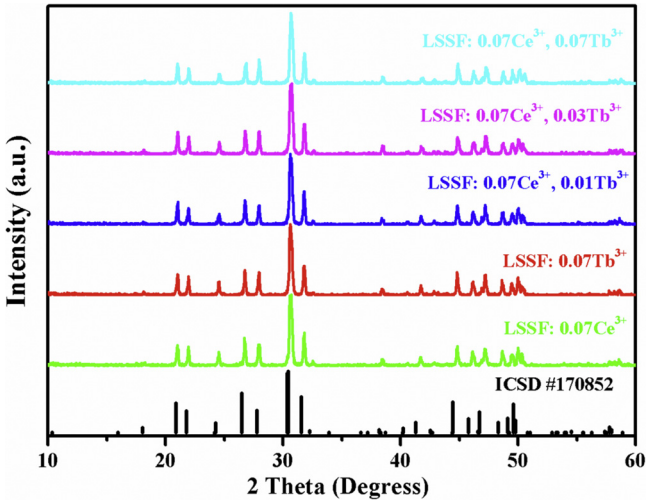

Fig. 2. X-ray diffraction patterns of $La_6Sr_4(SiO_4)_6F_2$:Ce^{3+}, Tb^{3+} samples and the standard data for $La_6Ba_4(SiO_4)_6F_2$ (ICSD card no. 170852) is shown as a reference.

main diffraction peak of the as-prepared LSSF: Ce^{3+}, Tb^{3+} samples shifted to higher diffraction angles compared to that of standard $La_6Ba_4(SiO_4)_6F_2$, which was caused by the Sr^{2+} substituting for Ba^2. Besides, the crystal parameters of the LSSF: $0.07Ce^{3+}$, yTb^{3+} (y = 0, 0.01, 0.03 and 0.07) and LSSF: $0.07Tb^{3+}$ phosphors were calculated by using the computer software Jade 5 as shown in Table 3. It can be seen that all the crystal parameters of the phosphors are closed to that that of $La_6Ba_4(SiO_4)_6F_2$. All the above results indicated that Ce^{3+} and Tb^{3+} ions can easily enter the crystal lattice of $La_6Ba_4(SiO_4)_6F_2$.

Fig. 3 illustrates the photoluminescence (PL) spectra of $La_{6-x}Sr_4(SiO_4)_6F_2$:xCe^{3+} (x = 0.01, 0.04, 0.07, 0.10, and 0.15) phosphors monitored by 282 nm, and the inset of Fig. 3 lists the Ce^{3+} content dependent emission intensity corresponding to the peaks at 419 nm. It can be easily found that the emission intensities of Ce^{3+} at 419 nm increased firstly with its concentration increasing, and reached the maximum at x = 0.07, then the emission intensity decreases, which was caused by the concentration quenching effect.

The photoluminescence excitation (PLE) and photoluminescence (PL) spectra of as-prepared $La_{5.93}Sr_4(SiO_4)_6F_2$:$0.07Ce^{3+}$ phosphor were illustrated in Fig. 4(a). The PLE spectrum monitored at 419 nm shows a broad absorption from 247 to 376 nm consisting of two broad bands centered at 282 and 349 nm

Table 3
The crystal parameters of the LSSF: $0.07Ce^{3+}$, yTb^{3+} (y = 0, 0.01, 0.03 and 0.07) and LSSF: $0.07Tb^{3+}$ phosphors.

Samples of LSSF: xCe^{3+}, yTb^{3+}	a (Å)	c (Å)	V (Å^3)
x = 0.07, y = 0	9.8556	7.3031	614.32
x = 0, y = 0.07	9.8603	7.3052	615.08
x = 0.07, y = 0.01	9.8628	7.3056	615.42
x = 0.07, y = 0.03	9.8664	7.3067	615.97
x = 0.07, y = 0.07	9.8709	7.3116	616.94

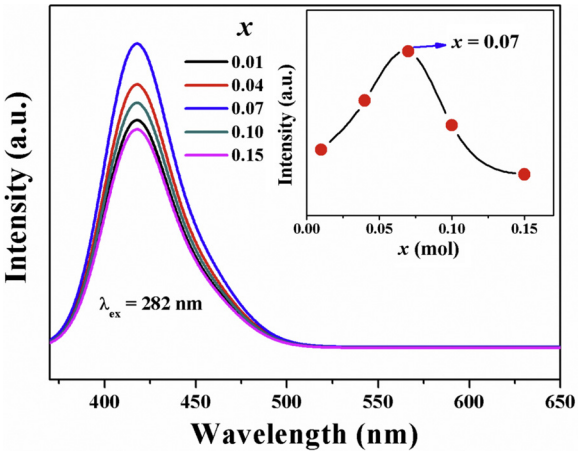

Fig. 3. The emission spectra of LSSF: xCe^{3+} (0.01, 0.04, 0.07, 0.10, and 0.15). The inset shows the dependence of the emission intensity on the concentration of Ce^{3+}.

attributed to 4f→5d transition of Ce^{3+} ions. The obvious excitation bands at 282 and 349 nm belong to Ce^{3+}(1) and Ce^{3+}(2) emission with seven- and nine-fold coordination, respectively. It is known to us that the ionic radii of coordinated Ce^{3+} ions in either seven- or nine-fold coordination are 1.196 and 1.07 Å similar to those (1.216 and 1.10 Å) of La^{3+} with seven- and nine-fold coordination, so Ce^{3+} ions can enter both La^{3+}(1) and La^{3+}(2) sites. Besides, it is more stable for Ce^{3+} to occupy the sites of La^{3+} with nine-fold coordination than that with seven-fold coordination. Thus, more Ce^{3+} occupy the La^{3+}(1) sites, and the bands at 282 nm, and the intensity of the bands at 282 nm are high than that at 349 nm. As shown in Fig. 4(a), the emission spectrum displays a broad band extending from 378 to 535 nm with a maximum at about 419 nm under the excitation wavelength of 282 nm. What is more, the PL spectrum can be divided into four dotted bands centered at about 398, 418, 433 and 460 nm by using Gaussian fitting, as marked by curve Ce1, Ce2, Ce3 and Ce4 shown in Fig. 4(a). In general, the emission spectrum for each site occupied by Ce^{3+} should contain two bands because of the electron transition from the lowest 5d excited state to $^2F_{7/2}$ and $^2F_{5/2}$ states, and the energy separation of the two bands is about 2000 cm^{-1}. Therefore, it is speculated that there may exists two types of Ce^{3+} luminescent centers in LSSF from the spectral profiles. As shown in the inset of Fig. 1, there are

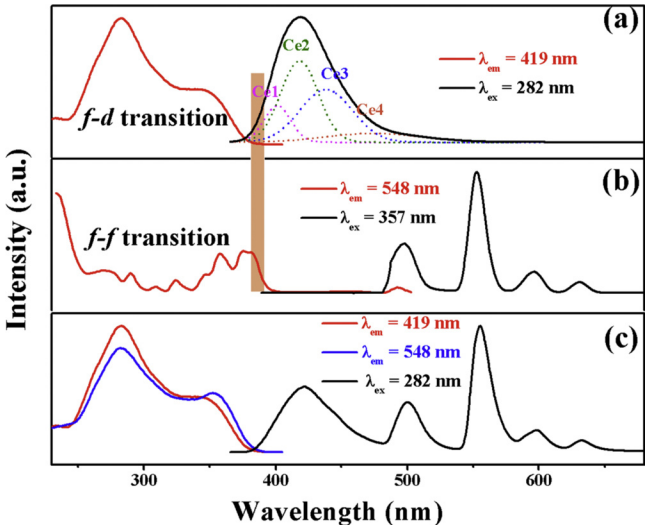

Fig. 4. PLE (left) and PL (right) spectra of $La_{5.93}Sr_4(SiO_4)_6F_2$:$0.07Ce^{3+}$ (a), $La_{5.93}Sr_4(SiO_4)_6F_2$:$0.07Tb^{3+}$ (b), and $La_6Sr_4(SiO_4)_6F_2$:$0.07Ce^{3+}$,$0.07Tb^{3+}$ (c) samples.

two types of nonequivalent crystallographic sites of La^{3+} (the 4*f* site and the 6 *h* site). Thus, it was concluded that bands Ce1 and Ce3 are the part of Ce^{3+} (1) emission with nine-coordination and Ce2 and Ce4 belong to Ce^{3+} (2) emission with seven-coordination. In addition, the energy gap between the bands Ce1 and Ce3 and the bands Ce2 and Ce4 can be calculated as 2030 cm^{-1} and 2184 cm^{-1} respectively, which are close to the theoretical value of 2000 cm^{-1}. As far as we know, the f–f absorption transitions of Tb^{3+} ions are forbidden transitions which are difficult to pump, and the PLE and PL spectra of Tb^{3+} singly doped LSSF sample are presented in Fig. 4(b). It can be found that only some narrow f–f transition lines in the region from 260 to 400 nm centered at 318, 347, 357, and 376 nm exists in the PLE spectrum of Tb^{3+} singly doped sample, which corresponds to the transitions from the $^7F_6$ ground state to the excited states of Tb^{3+}. As presented in Fig. 4(b), the PL spectrum under the excitation of 357 nm shows the typical characteristic $^5D_4$–^7F_J (J = 6, 5, 4, and 3) transitions of Tb^{3+} ions, which are situated at about 497, 548, 593, and 628 nm. In general, Ce^{3+} ions can be co-doped as sensitizers to transfer excitation energy to Tb^{3+} ions to enhance the absorption intensity in the n-UV region for the Tb^{3+} emission [32]. Besides, it can be also found that there is an overlap between the emission band of Ce^{3+} and the f-f absorptions of Tb^{3+} in the region of 381–392 nm in Fig. 4(a) and (b), which indicates the possible resonance type energy transfer from Ce^{3+} to Tb^{3+} in LSSF crystal lattice. The energy transfer can be confirmed by the PLE and PL spectra of LSSF:0.07Tb^{3+} in Fig. 4(b). The PLE spectrum monitored at the emission of Tb^{3+} (548 nm) is consistent to that monitored at the emission of Ce^{3+} (419 nm) except for the difference in relative intensity in Fig. 4(c). Moreover, the presence of both a blue band of the Ce^{3+} ions at 419 nm and some emission lines of the Tb^{3+} ions in the PL spectrum of LSSF:0.07Ce^{3+}, 0.07Tb^{3+} phosphor monitored at 282 nm further suggests that LSSF:0.07Ce^{3+}, 0.07Tb^{3+} can serve as the green emitting phosphor for n-UV LEDs on the basis of the energy transfer from Ce^{3+} to Tb^{3+}.

In order to further study the energy transfer process between the Ce^{3+} and Tb^{3+} ions in the LSSF host lattice, a series of LSSF:Ce^{3+}, Tb^{3+} phosphors were prepared. Fig. 5 presents the emission spectra of $La_{5.93-y}Ba_4(SiO_4)_6F_2$:0.07$Ce^{3+}$, yTb^{3+} (y = 0, 0.01, 0.03, 0.05, 0.07) phosphors under the excitation of 282 nm. As shown in Fig. 5, a characteristic broad emission of Ce^{3+} ions and several sharp emission lines of Tb^{3+} ions are observed in $La_{5.93-y}Ba_4(SiO_4)_6F_2$:0.07$Ce^{3+}$, yTb^{3+} phosphors except for the PL spectra of $La_{5.93}Ba_4(SiO_4)_6F_2$:0.07$Ce^{3+}$. Besides, the relative emission intensities of the Ce^{3+} ions decreased remarkably with increasing Tb^{3+} concentration, while the relative emission intensities of Tb^{3+} increased, which should be caused by the enhancement of energy transfer from the Ce^{3+} ions to Tb^{3+} ions.

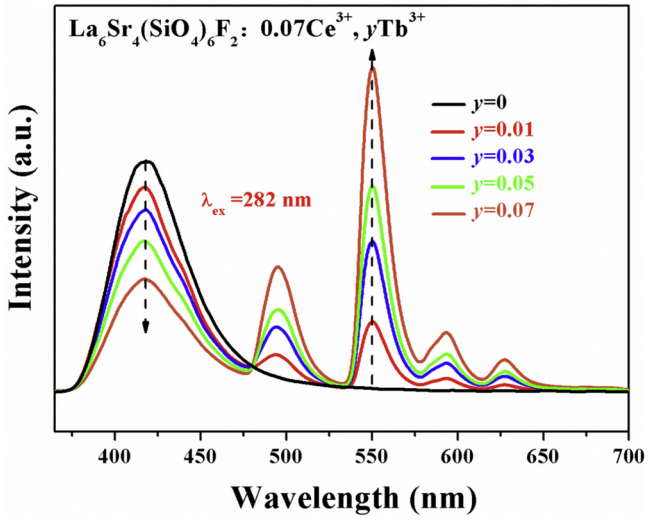

Fig. 5. The emission spectra of $La_6Sr_4(SiO_4)_6F_2$: 0.07Ce^{3+}, yTb^{3+} phosphors (λ_{ex} = 282 nm), and the inset shows the variation of Ce^{3+} emission (419 nm) and Tb^{3+} emission (548 nm) as a function of Ce^{3+} concentration.

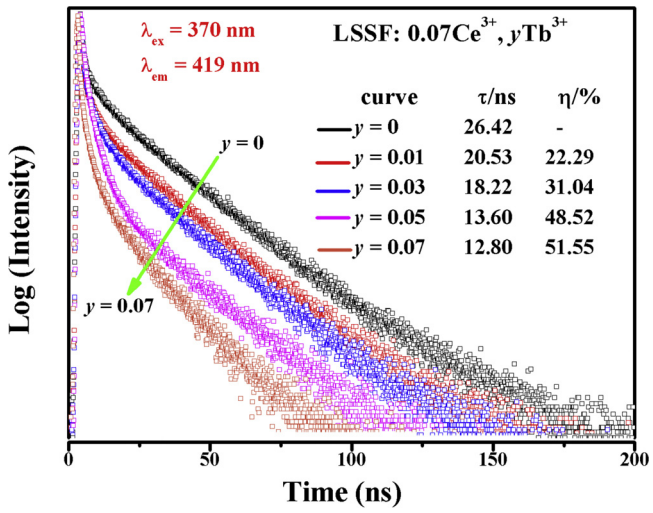

Fig. 6. Decay curves and lifetime of Ce^{3+}, as well as the energy transfer efficiency from Ce^{3+} to Tb^{3+} in $La_6Sr_4(SiO_4)_6F_2$:0.07Ce^{3+},yTb^{3+} (0.01, 0.03, 0.05, and 0.07) phosphors (excited at 370 nm, monitored at 413 nm) at room temperature.

It can be found that the decay curves of Ce^{3+} ions are non-exponential, the decay process of theses samples are characterized by average lifetime (τ), which can be defined by using Eq. (1) [33].

$$\tau = \frac{\int_0^\infty I(t)tdt}{\int_0^\infty I(t)dt} \quad (1)$$

where $I(t)$ is the luminescence intensity at time t after the cutoff of the excitation light. According to Eq. (1), the lifetimes of Ce^{3+} ions were determined to be 26.42, 20.53, 18.22, 13.60, and 12.80 ns for LSSF:0.07Ce^{3+}, yTb^{3+} samples (y = 0, 0.01, 0.03, 0.05, and 0.07). It can be observed that the decay lifetime for Ce^{3+} was found to decrease with the concentration of Tb^{3+} ions increases, which provided a strong evidence for the energy transfer from Ce^{3+} ions to Tb^{3+} ions. The energy transfer efficiency η_{Ce-Tb} can be expressed using Eq. (2) [34]:

$$\eta Ce - Tb = 1 - \tau_S/\tau_0 \quad (2)$$

where τ_S and τ_{S0} represent the lifetimes of Ce^{3+} in the presence and absence of Tb^{3+}, respectively. Based on the values of the lifetimes calculated according to Eq. (1), the energy transfer efficiency from the sensitizer Ce^{3+} to the activator Tb^{3+} was calculated according to Eq. (2), which are given in the inset of Fig. 6. It can be seen that the value of η_{Ce-Tb} increased gradually with increasing contents of Tb^{3+}, and reached the maximum at 51.55% when y = 0.07.

The critical energy transfer distance R_C between Ce^{3+} and Tb^{3+} ions can be estimated by using concentration quench Eq. (3) proposed by Blasse [35]:

$$R_C \approx 2\left[\frac{3V}{4\pi x_c N}\right]^{1/3} \quad (3)$$

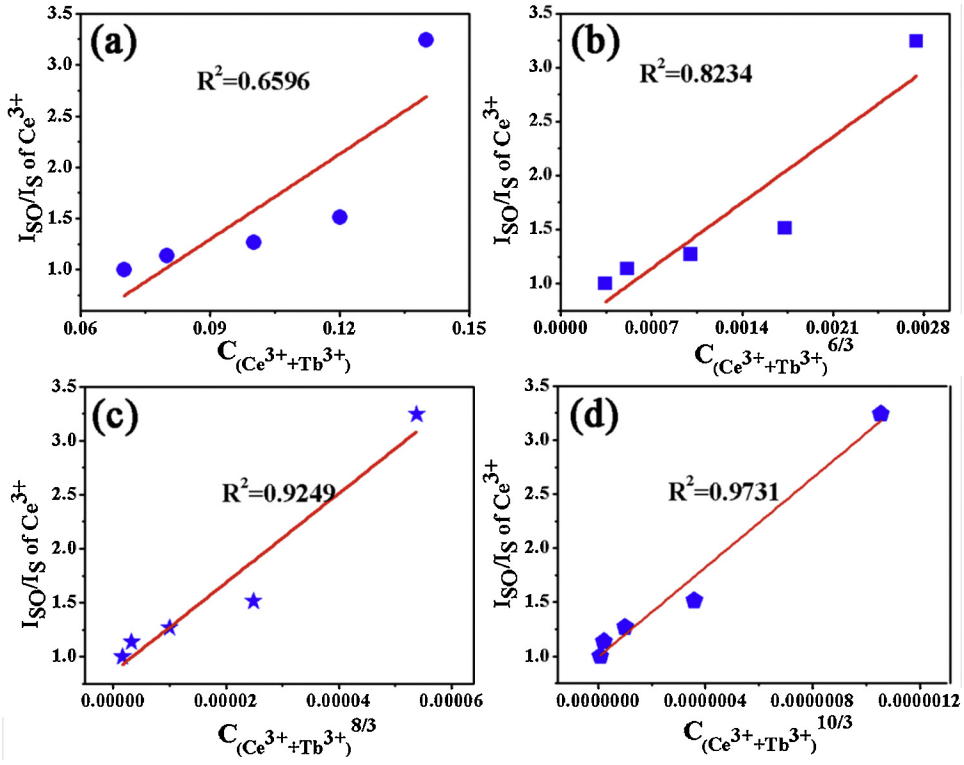

Fig. 7. Dependence of I_{S0}/I_S of Ce^{3+} on (a) $C_{(Ce^{3+}+Tb^{3+})}$; (b) $C_{(Ce^{3+}+Tb^{3+})^{6/3}}$; (c) $C_{(Ce^{3+}+Tb^{3+})^{8/3}}$; (d) $C_{(Ce^{3+}+Tb^{3+})^{10/3}}$.

where V is the volume of the crystallographic unit cell, x_c is the critical concentration (quenching concentration) and N is the number of lattice sites in the unit cell that can be occupied by activator ions. Here, for $La_6Sr_4(SiO_4)_6F_2$, it exists ten number of host cations in one unit cell. Thus, N was determined as 10. As shown in Fig. 3, the emission intensities of Ce^{3+} at 419 nm increased firstly with its concentration increasing, and maximized at $x = 0.07$, and then decreased with increasing Ce^{3+} content caused by the concentration quenching effect. Thus, x_c is 0.07 as critical concentration. Besides, the volume of $La_{5.93}Ce_{0.07}Sr_4(SiO_4)_6F_2$ is 614.32 Å^3 as shown in Table 3. Based on Eq. (3), the critical distances of energy transfer for Ce^{3+} to Tb^{3+} ions are turned out to be about 11.878 Å ($x_c = 0.07$). The quantitative theories of Eq. (3) are based on resonance transfer by electric multipole interaction or exchange interaction. Non-radiative energy transfer plays an important role in the luminescence of oxidic phosphors, the Eq. (3) proposed by Blasse usually used for determining the possibility of electric multipole interaction or exchange interaction. In general, if the critical distance of energy transfer is larger than 5 Å the exchange interaction will be ineffective, and only a multipolar interaction will be important. Thus, the energy transfer from Ce^{3+} to Tb^{3+} in $La_6Sr_4(SiO_4)_6F_2$ may take place via multipolar interaction, which was because that the R_C value is 11.878 Å larger than 5 Å. According to Dexter's energy transfer expressions of multipolar interaction and Reisfeld's approximation, Eq. (4) can be used as [36]:

$$\eta_{S0}/\eta_S \propto C \text{ and } \eta_{S0}/\eta_S \propto C^{n/3} \quad (4)$$

where η_S and η_{S0} are the luminescence quantum efficiency of Ce^{3+} in the presence and absence of Tb^{3+}, and C is the total content of Ce^{3+} and Tb^{3+}. Besides, the value of n can be 6, 8, and 10, respectively. In general, the values η_{S0}/η_S can be replaced approximately by the ratio of the related luminescence intensities (I_{S0}/I_S) as equation (5)

$$I_{S0}/I_S \propto C \text{ and } I_{S0}/I_S \propto C^{n/3} \quad (5)$$

The $I_{S0}/I_S \propto C$ and $I_{S0}/I_S \propto C^{n/3}$ plots are shown in Fig. 7(a)–(d). As is known to us, the relationship of $(I_{S0}/I_S) \propto C$ corresponds to the exchange interaction, and $n = 6$, 8, and 10 for dipole–dipole (d–d), dipole–quadrupole (d–q), and quadrupole–quadrupole (q–q) interactions, respectively [37]. It can be found that the fitting factors of R values of the relationship of $(I_{S0}/I_S) \propto C$ is smaller than those of $I_{S0}/I_S \propto C^{n/3}$ indicating the exchange interaction will be ineffective in LSSF, which is caused by the R_C value 11.878 Å (more than 5). A liner relation can be observed when $n = 10$, which suggests that the energy transfer from Ce^{3+} to Tb^{3+} in LSSF host is

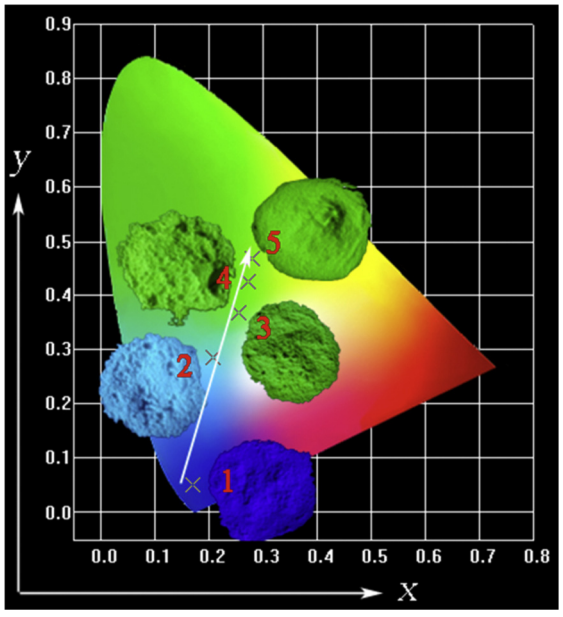

Fig. 8. CIE chromaticity coordinates (x_{CIE},y_{CIE}) of LSSF: $0.07Ce^{3+}$, yTb^{3+} (0.01, 0.03, 0.05, and 0.07) samples upon 282 nm excitation and the digital photos of the samples under 365 nm UV lamp excitation.

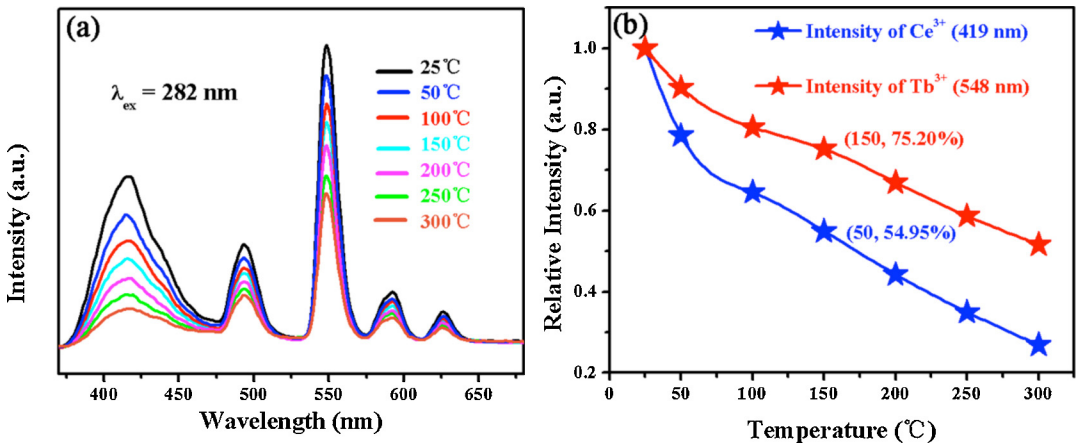

Fig. 9. a The temperature-dependent emission spectra for LSSF:0.07Ce^{3+}, 0.07Tb^{3+} samples under 282 nm excitation; Fig. 9(b) The relative emission intensities centered at 419 (Ce^{3+}) and 548 nm (Tb^{3+}) as a function of temperature.

Table 4
Comparison of CIE Chromaticity Coordinates for $La_6Sr_4(SiO_4)_6F_2$:0.07Ce^{3+}, yTb^{3+} (0.01, 0.03, 0.05, and 0.07) phosphors (λ_{ex} = 365 nm).

No. of points in CIE diagram	Sample compositions of $La_{5.93-y}Sr_4(SiO_4)_6F_2$:0.07$Ce^{3+}$, yTb^{3+}	CIE (x_{CIE},y_{CIE})
1	y = 0	(0.169,0.049)
2	y = 0.01	(0.208,0.285)
3	y = 0.03	(0.256,0.367)
4	y = 0.05	(0.273,0.424)
5	y = 0.07	(0.279,0.467)

dominated by the quadrupole–quadrupole (q–q) mechanism by comparing the fitting factors of R values.

The x_{CIE} and y_{CIE} values of CIE chromaticity coordinates and CIE chromaticity diagram were measured and calculated through its PL spectrum, and the CIE chromaticity coordinates (x_{CIE},y_{CIE}) of LSSF: 0.07Ce^{3+}, yTb^{3+} (y = 0, 0.01, 0.03, 0.05, and 0.07) samples upon 282 nm excitation are shown in Table 4 and Fig. 8. The inset in Fig. 8 also shows a series of digital photos of LSSF:0.07Ce^{3+}, yTb^{3+} phosphors. With Ce^{3+} concentration fixed at x = 0.07, the emitting color of the phosphors shift gradually from blue region (0.169, 0.049) to bluish-green region (0.208, 0.285) and eventually to green region (0.279, 0.467) with an increase of Tb^{3+} concentration. Therefore, the as-prepared samples have great potential application as green emitting phosphor for n-UV LEDs.

As we know, thermal stability of phosphor is very important for the potential applications in high-power LEDs. The temperature-dependent emission spectra for the selected LSSF:0.07Ce^{3+}, 0.07Tb^{3+} samples under 282 nm excitation are presented in Fig. 9(a) and (b) shows the relative emission intensities centered at 419 (Ce^{3+}) and 548 nm (Tb^{3+}) as a function of temperature. It can be obviously seen that both the PL intensities at 419 and 548 nm decrease with increasing temperature. It is known to us that phosphors used for LEDs are better to exhibit strong thermal quenching resistance to sustain their emission efficiency up to 150°C, which was because that the temperature of a LED package may rise during LED operation. The relative PL intensities of LSSF:0.07Ce^{3+}, 0.07Tb^{3+} decreased to 54.95% (419 nm) and 75.20% (548 nm) of the initial PL intensity with the temperature rising from room temperature to 150 °C, which indicated that LSSF:0.07Ce^{3+}, 0.07Tb^{3+} phosphor has a high thermal stability.

4. Conclusions

In summary, a series of single-phase LSSF:Ce^{3+},Tb^{3+} phosphors were prepared by a high temperature solid-state reaction. The photoluminescence spectra of the samples show a broad blue band emission of Ce^{3+} at 419 nm and the green peak emission of Tb^{3+}, respectively. The emission color of the as-prepared phosphors can be tuned appropriately from blue region (0.169, 0.049) to bluish-green region (0.208, 0.285) and eventually to green region (0.279, 0.467) by adjusting the concentration of Tb^{3+}. The energy transfer from Ce^{3+} to Tb^{3+} in the $La_6Sr_4(SiO_4)_6F_2$ host has been demonstrated to be quadrupole–quadrupole (q–q) mechanism. The critical distances R_C of energy transfer were calculated by concentration quenching and turned out to be about 11.878 Å (x_c = 0.07). The selected LSSF:0.07Ce^{3+}, 0.07Tb^{3+}phosphor shows high thermal quenching temperature. All above results indicate that LSSF:Ce^{3+},Tb^{3+} could be used as a green emitting phosphor for n-UV w-LEDs.

Acknowledgment

This present work is supported by the National Natural Science Foundations of China (Grant No. 41172053).

References

[1] X. Zhang, L. Huang, F. Pan, M. Wu, J. Wang, Y. Chen, Q. Su, Highly thermally stable single-component white-emitting silicate glass for organic-resin-free white-light-emitting diodes, ACS Appl. Mater. Interfaces 6 (2014) 2709–2717.
[2] I.S. Sohn, S. Unithrattil, W.B. Im, Stacked quantum dot embedded silica film on a phosphor plate for superior performance of white light-emitting diodes, ACS Appl. Mater. Interfaces 6 (2014) 5744–5748.
[3] L. Qin, Y.L. Huang, T.J. Tsuboi, J.S. Hyo, The red-emitting phosphors of Eu^{3+}-activated $MR_2(MoO_4)_4$ (M = Ba, Sr, Ca; R = La^{3+}, Gd^{3+}, Y^{3+}) for light emitting diodes, Mater. Res. Bull. 47 (2012) 4498–4502.
[4] C.H. Huang, T.M. Chen, A novel single-composition trichromatic white-light $Ca_3Y(GaO)_3(BO_3)_4$: Ce^{3+}, Mn^{2+}, Tb^{3+} phosphor for UV-light emitting diodes, J. Phys. Chem. C 115 (2011) 2349–2355.
[5] H.S. Jang, I.W. Bin, D.C. Lee, D.Y. Jeon, S.S. Kim, Enhancement of red spectral emission intensity of $Y_3Al_5O_{12}$: Ce^{3+} phosphor via Pr co-doping and Tb substitution for the application to white LEDs, J. Lumin. 126 (2007) 371–377.
[6] S.S. Novosad, I.S. Novosad, L.V. Kostyk, Recombination processes in the $Y_3Al_5O_{12}$: Ce^{3+} scintillator, Inorg. Mater. 5 (2008) 515–519.
[7] Y. Chen, M. Gong, G. Wang, Q. Su, High efficient and low color-temperature white light-emitting diodes with $Tb_3Al_5O_{12}$: Ce^{3+} phosphor, Appl. Phys. Lett. 91 (2007) 71117–71119.
[8] A.A. Setlur, W.J. Heward, Y. Gao, A.M. Srivastava, R.G. Chandran, M.V. Shankar, Crystal chemistry and luminescence of Ce^{3+}-doped $Lu_2CaMg_2(Si,Ge)_3O_{12}$ and its use in LED based lighting, Chem. Mater. 18 (2006) 3314–3322.
[9] X. Chen, P.P. Dai, X.T. Zhang, C. Li, S. Lu, X.L. Wang, Y. Jia, Y.C. Liu, Color-tunable emission and energy transfer in $Ca_3Gd_7(PO_4)(SiO_4)_5O_2$: Ce^{3+}/Tb^{3+}/Mn^{2+} phosphors, Inorg. Chem. 51 (2012) 11655–11664.
[10] X.G. Zhang, L.Y. Zhou, Q. Pang, J.N. Shi, M.L. Gong, Tunable luminescence and Ce^{3+}→Tb^{3+}→Eu^{3+} energy transfer of broadband-excited and narrow line red emitting Y_2SiO_5: Ce^{3+}, Tb^{3+}, Eu^{3+} phosphor, J. Phys. Chem. C 118 (2014) 7591–7598.

[11] C.F. Guo, Z. Yang, J. Yu, J.H. Jeong, Photoluminescence and efficient energy transfer from Ce^{3+} to Tb^{3+} or Mn^{2+} in $Ca_9ZnLi(PO_4)_7$ host, Appl. Phys. A Mater. Sci. Process 108 (2012) 569–576.
[12] J.S. Cho, K.Y. Jung, Y.C. Kang, Yolk–shell structured Gd_2O_3: Eu^{3+} phosphor prepared by spray pyrolysis: the effect of preparation conditions on microstructure and luminescence properties, Phys. Chem. Chem. Phys. 17 (2015) 1325–1331.
[13] Y.T. Li, X.H. Liu, Sol–gel synthesis, structure and luminescence properties of Ba_2ZnMoO_6: Eu^{3+} phosphors, Mater. Res. Bull. 64 (2015) 88–92.
[14] S.S. Hu, W.J. Tang, Synthesis and luminescence properties of Eu^{2+}- and Mn^{2+}-activated $Mg_{21}Ca_4Na_4(PO_4)_{18}$ phosphors, J. Mater. Sci. 48 (2013) 5840–5845.
[15] Y. Li, Y. Shi, Q. Zhu, H. Li, X. Wang, Y. Wang, A Single-component white-emitting $CaSr_2Al_2O_6$: Ce^{3+}, Li^+, Mn^{2+} phosphor via energy transfer, Inorg. Chem. 53 (2014) 7668–7675.
[16] B. Hüttl, Luminescence properties of SrS: Ce^{3+}, J. Appl. Phys. 78 (1995) 7282–7288.
[17] T.J. Lee, Visible quantum cutting through downconversion in green-emitting K_2GdF_5: Tb^{3+} phosphors, Appl. Phys. Lett. 89 (2006) 131121–131123.
[18] D. Jia, Green phosphorescence of $CaAl_2O_4$: Tb^{3+}, Ce^{3+} through persistence energy transfer, Appl. Phys. Lett. 80 (2002) 1535–1537.
[19] Y.K. Tosaka, S.D. Adachi, P. He, Photoluminescence properties and energy-level diagrams in (Ce^{3+}, Tb^{3+})-codoped KCl green phosphor, J. Lumin. 156 (2014) 157–163.
[20] H.K. Liu, Q.F. Guo, L.B. Liao, Z.G. Xia, Synthesis and energy transfer studies of Eu^{2+} and Mn^{2+} co-doped $Sr_{3.45}Y_{6.5}O_2(PO_4)_{1.5}(SiO_4)_{4.5}$ phosphor, Opt. Commun. 309 (2013) 64–67.
[21] H.K. Liu, Y.Y. Zhang, L.B. Liao, Q.F. Guo, L.F. Mei, Synthesis, broad-band absorption and luminescence properties of blue-emitting phosphor $Sr_8La_2(PO_4)_6O_2$: Eu^{2+} for n-UV white-light-emitting diodes, Ceram. Int. 40 (2014) 13709–13713.
[22] F. Zhang, T. Lan, W.J. Tang, Tunable photoluminescence properties of $Ca_8NaLa(PO_4)_6F_2$: Eu^{2+}, Mn^{2+} phosphor under UV excitation, Mater. Res. Bull. 64 (2015) 128–133.
[23] R.J. Yu, H.J. Li, H.L. Ma, C.F. Wang, H. Wang, A new blue-emitting phosphor of Ce^{3+}-activated fluorosilicate apatite $Ba_2Y_3[SiO_4]_3F$, J. Am. Chem. Soc. 97 (2014) 1151–1156.
[24] R.Y. Mi, C.L. Zhao, Z.G. Xia, Synthesis, structure, and tunable luminescence properties of novel $Ba_3NaLa(P_{O4})_3F$: Eu^{2+}, Mn^{2+} phosphors, J. Am. Chem. Soc. 97 (2014) 1802–1808.
[25] M.D. Que, Z.P. Ci, Y.H. Wang, G. Zhu, S.Y. Xin, Y.R. Shi, Q. Wang, Crystal structure and luminescence properties of a cyan emitting $Ca_{10}(SiO_4)_3(SO_4)_3F_2$: Eu^{2+} phosphor, CrystEngComm 15 (2013) 6389–6394.
[26] Q.F. Guo, L.B. Liao, Z.G. Xia, Luminescence properties and energy transfer in $La_6Ba_4(SiO_4)_6F_2$: Ce^{3+},Tb^{3+} phosphors, J. Lumin. 145 (2014) 65–70.
[27] C. Peng, G.G. Li, Z.Y. Hou, M.M. Shang, J. Lin, Electrospinning synthesis and luminescent properties of one-dimensional $Ca_2Gd_8(SiO_4)_6O_2$: Eu^{3+} microfibers and microbelts, Mater. Chem. Phys. 136 (2012) 1008–1014.
[28] K. Li, D.L. Geng, M.M. Shang, Y. Zhang, H.Z. Lian, J. Lin, Color-tunable luminescence and energy transfer properties of $Ca_9Mg(PO_4)_6F_2$: Eu^{2+}, Mn^{2+} phosphors for UV-LEDs, J. Phys. Chem. C 118 (2014) 11026–11034.
[29] Bruker AXS TOPAS V4: General Profile and Structure Analysis Software for Powder Diffraction Data. – User's Manual, Bruker AXS, Karlsruhe, Germany, 2008.
[30] X. Gong, Y. Lin, Y. Chen, Z. Huang, Y. Huang, Z. Luo, Syntheses, structure, and characterization of crystal $La_6Ba_4(SiO_4)_6F_2$, a promising laser host, Chem. Mater. 17 (2005) 1135–1138.
[31] R.D. Shannon, Revised effective ionic radii and systematic studies of interatomie distances in halides and chaleogenides, Acta. Cryst. A 32 (1976) 751–767.
[32] M.J. Xu, L.X. Wang, D.Z. Jia, F.H. Le, Luminescence properties and energy transfer investigations of $Zn_2P_2O_7$: Ce^{3+}, Tb^{3+} phosphor, J. Lumin. 158 (2015) 125–129.
[33] L.G. Van Uitert, An empirical relation fitting the position in energy of the lower d-band edge for Eu^{2+} or Ce^{3+} in various compounds, J. Lumin. 29 (1984) 1–9.
[34] N. Guo, Y.H. Zheng, Y.C. Jia, H. Qiao, H.P. You, Warm-white-emitting from Eu^{2+}/Mn^{2+}-Codoped $Sr_3Lu(PO_4)_3$ phosphor with tunable color tone and correlated color temperature, J. Phys. Chem. C 116 (2012) 1329–1334.
[35] G. Blasse, Energy transfer in oxidic phosphors, Philips Res. Rep. 24 (1969) 131–136.
[36] D. Dexter, A theory of sensitized luminescence in solids, J. Chem. Phys. 21 (1953) 836–850.
[37] S.H. Miao, Z.G. Xia, J. Zhang, Q.L. Liu, Increased Eu^{2+} content and codoping Mn^{2+} induced tunable full-color emitting phosphor $Ba_{1.55}Ca_{0.45}SiO_4$: Eu^{2+}, Mn^{2+}, Inorg. Chem. 53 (2014) 10386–10393.